# Thermodiffusion of repulsive charged nanoparticles - Interplay between single-particle and thermoelectric contributions.

*R. Cabreira Gomes, A. Ferreira da Silva, M. Kouyaté, G. Demouchy, G. Mériguet, R. Aquino, E. Dubois, S. Nakamae, M. Roger, J. Depeyrot and R. Perzynski*

ELECTRONIC SUPPLEMENTARY INFORMATION

## 1 Osmotic pressure and compressibility of moderately concentrated magnetic fluids

### 1.1 Effective hard spheres

We have checked with a large number of ionic Magnetic Fluid dispersions, similar to the ones of the main paper, that the following Carnahan-Starling equation of the osmotic pressure $\Pi$ and compressibility $\chi$ as a function of the effective volume fraction $\Phi_{\rm eff} = \Phi\left(1+\frac{2\kappa^{-1}}{d_{\rm NP}}\right)$ can be used to describe the measured $\Pi$ and $\chi$ for dispersions of NPs in strong interparticle repulsion.

$$\Pi = \frac{kT\ \Phi}{V_{\rm NP}}\ \frac{1+\Phi_{\rm eff}+\Phi_{\rm eff}^2-\Phi_{\rm eff}^3}{(1-\Phi_{\rm eff})^3}$$

$$\chi = \frac{(1-\Phi_{\rm eff})^4}{1+4\Phi_{\rm eff}+4\Phi_{\rm eff}^2-4\Phi_{\rm eff}^3+\Phi_{\rm eff}^4}.$$

This formalism is extensively presented in sections 2 and 3 of the main paper.

As the experiments necessary to check these expressions are long, heavy and expensive, the presented data have been gathered from several of our experiments dedicated to different questions, done over the years on several dispersions.

Determinations of osmotic pressure $\Pi$ as a function of volume fraction $\Phi$ have been obtained by osmotic stress and various chemical titrations. They are very long and expensive.

Compressibility determinations have been done through a very large number of Small Angle Scattering experiments, using both Neutrons at LLB (Saclay – France) and ILL (Grenoble – France) and X-rays at SOLEIL (Gif sur Yvette – France) and ESRF (Grenoble – France). These experiments are not of easy access and cannot be asked for just a sample characterization. Thus all these probing cannot be realized each time for all the samples used in the numerous experiments involving Magnetic Fluids.

### 1.2 Sample preparation

The routine way of preparing samples with a well characterized volume fraction and ionic strength is to prepare by osmotic stress a substantial quantity of an intermediate sample in order to concentrate the NPs and to reduce the ionic strength with respect to the one directly issued from the chemical synthesis. To choose the conditions of preparation of this intermediate sample, we indeed use our knowledge of $\Pi = f(\Phi)$ variations as a function of the NPs characteristics, of the nature of surface coating and of the concentration of free ions. Series of samples for experiments, such as these presented in the main paper, are then obtained by careful dilution of the intermediate sample with adapted solutions to reach the desired concentrations and ionic strengths.

Series of Magnetic Fluids based on NP's comparable to that of the main paper have been prepared at given ionic strengths (or pH values) by osmotic stress and probed by Small Angle Scattering.

#### 1.2.1 Osmotic pressure

The initial Magnetic Fluid directly obtained from the chemical synthesis process is put in a dialysis-tubing (Spectra/Por membrane 6-8 kDa) inside a compression bath much larger than the volume of the dialysis tubing (clipped at both ends to form a bag). In the bath, polymer chains of polyethylene glycol (PEG) of molecular mass $M_w = 2\times10^4$ g mol$^{-1}$ are used to control the

osmotic pressure and small ions to control pH and ionic strength. While water and small ions can pass through the membrane of the dialysis bag, neither the NP's (inside the bag) nor the polymer outside can cross the membrane. At thermodynamic equilibrium (after several weeks), the osmotic pressure $\Pi$ of the NPs in the bag equals that of the external polymer, which is fixed by the polymer concentration. The Magnetic Fluid, at controlled ionic strength (or pH), is then extracted from the bag to determine its volume fraction $\Phi$ either by chemical titration or by density measurement.

### 1.2.2 Compressibility

Afterwards the obtained Magnetic Fluid can be easily diluted at known concentrations and ionic strengths (or pH). Thus in routine preparation of acidic samples, a sample at a slightly larger pH than the desired one is usually prepared, in order to be able to dilute it accurately to reach the wanted concentration and ionic strength (or pH). In the case of citrate coated NPs, in routine preparation, a concentrated sample at the desired $[\text{cit}]_{\text{free}}$ concentration is prepared, it is then diluted with a solution at the same $[\text{cit}]_{\text{free}}$.

Series of Magnetic Fluids based on the same NPs at various concentrations and ionic strengths prepared in that way, have been probed by Small Angle Scattering, either by Neutron scattering (SANS) (either at PAXY - LLB - Saclay - France or D22 - ILL - Grenoble - France) or by X-ray scattering (SAXS) (either at ID02 - ESRF - Grenoble - France or at SWING - SOLEIL - Gif sur Yvette - France). It allows the determination of the form factor of the NPs from a Zimm-Plot and the structure factor $S(q)$ of the dispersions. The compressibility is then obtained from the limit of $S(q)$ at very low scattering vector[1–3].

## 1.3 Citrate-coated NPs

In the case of NPs coated with citrate groups, both the compressibility and the osmotic pressure depend on the concentration of free citrate species – see Fig. 1 of the main paper – and their detailed fitting in section 2.2 of the main paper.

## 1.4 Hydroxyl-coated NPs

In the case of NPs coated with hydroxyl groups, both the compressibility and the osmotic pressure depend on the pH of the dispersion (and eventually on added ionic strength). We show only results at pH = 2 and 3, without added ionic strength, with NP's characteristics close to the ones of the main paper.

The main figure 1 of E.S.I. collects the $\Phi$-dependence of the compressibility $\chi$ at pH =2 (far from the glass transition) for three samples (B8, B9 and B10 - see Table 1 of E.S.I. - very similar to the acidic ones of main paper), together with its adjustment $\chi_{CS}$ by the Carnahan-Starling model using $\Phi_{\text{eff}} = 4.5\Phi$. The inset of Figure 2 presents the osmotic pressure at pH= 2 and 3 of sample B8 in a reduced representation $\Pi V_{\text{NP}}/\Phi kT$ as a function of $\Phi_{\text{eff}}$ using $V_{\text{NP}} = \frac{\pi}{6} d_{\text{NP}}^3 = \frac{\pi}{6} \langle d_{\text{mag}}^3 \rangle$. Both quantities are well adjusted with the Carnahan-Starling model far from the glass transition (typically for $\Phi_{\text{eff}}$ up to $\sim 0.36$).

# 2 Nanoparticle characterizations

## 2.1 Magnetic characteristics

The magnetic NP characteristics (see Tables 1 and 2 of E.S.I.) are obtained by magnetization measurements at room temperature. $m_{\text{s}}$ is the NP material magnetization, $d_{\text{mag}}^0$ is the median diameter and $\sigma$ is the polydispersity index of the log-normal distribution of NP magnetic diameters (for small $\sigma$, the standard deviation of the diameter distribution is close to $\sigma d_{\text{mag}}^0$). $m_{\text{s}}$,

**Table 1** Characteristics of the samples probed in Figure 1 of Electronic Supporting Information.

| NPs | Core Ferrite | Surf. Groups | pH | $d_{\text{mag}}^0(nm)$ | $\sigma$ | $d_{\text{NP}}$ (nm) |
|---|---|---|---|---|---|---|
| B8 | $\gamma$-$Fe_2O_3$ | Hydroxyl | 2 & 3 | 10.5 | 0.3 | 12 |
| B9 | $CoFe_2O_4$ | Hydroxyl | 2 | 9.4 | 0.36 | 11.4 |
| B10 | $\gamma$-$Fe_2O_3$ | Hydroxyl | 2 | 9.2 | 0.4 | 11.7 |

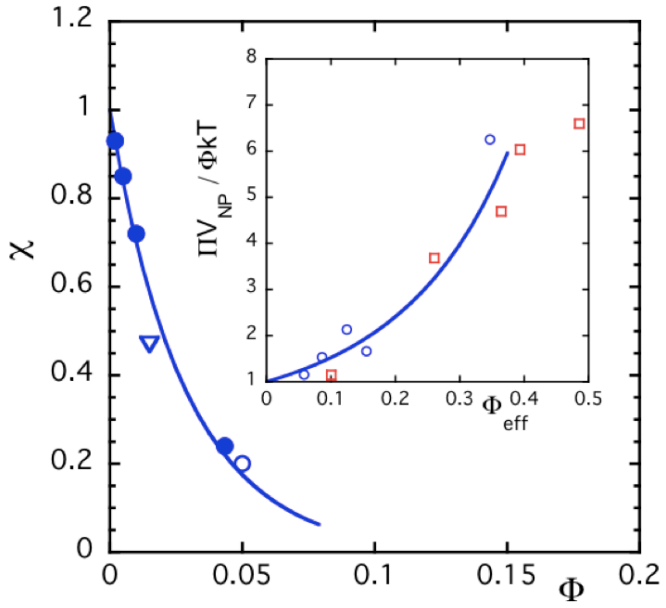


**Figure 1** Main figure : Adjustment (full line) by the Carnahan-Starling model of the volume fraction dependence at pH = 2 of the compressibility $\chi$ of samples B8 (○), B9 (▽) and B10 (●) of table 1 of S.I.; Inset : reduced representation of the osmotic pressure $\Pi V_{NP}/\Phi kT$ as a function of $\Phi_{eff}$ of sample B8 at pH = 2 (○) and 3 (□) using $V_{NP} = \frac{\pi}{6} d_{NP}^3$ (see Table 1 and section 2.1 of E.S.I.). - color on line

$d_{mag}^0$ and $\sigma$ are experimentally determined from the adjustment of the dispersion magnetization at a low volume fraction $\Phi_{dil}$ by a Langevin function weighted by the log-normal distribution of diameters[4]. The NP saturation magnetization $m_s$ is given by $M^{sat}/\Phi_{dil}$, with $M^{sat}$ the saturation magnetization of the different samples at $\Phi_{dil}$. The NP diameter $d_{NP}$ is here assimilated to $\sqrt[3]{\langle d_{mag}^3 \rangle}$ (see Table 2).

The dipolar interaction parameter $\Psi_{dd}$ (defined as $\Psi_{dd} = \frac{\mu_0}{kT} m_s^2 \frac{\pi}{6} d_{LF}^3$ with $d_{LF} = \sqrt[3]{\langle d^6 \rangle / \langle d^3 \rangle}$ the low-field-averaged diameter) is experimentally determined by the measurement of the initial magnetic susceptibility $\chi_{magn}^0$ at a low volume fraction $\Phi_{dil}$ [1,2] through $\Psi_{dd} = 3\chi_{magn}^0/\Phi_{dil}$. Table 2 presents both the parameter $\Psi_{dd}$ characteristic of the size distribution of the NPs and the more standard magnetic dipolar parameter $\lambda$ of the dispersion. $\lambda$ is the ratio of the dipolar energy to thermal one. It is here calculated at the maximal volume fraction of the probed samples $\Phi_{max}$; namely $\lambda_{max} = \Psi_{dd}\Phi_{max}/4\pi$. It is always smaller than 1, a zero field chaining of the nanoparticles being thus impossible for these NPs.

## 2.2 Optical characteristics

### 2.2.1 Optical absorption and optical index of the ferrofluid dispersions

Table 3 of E.S.I. presents the experimental values of the optical absorption coefficient and of the optical index of the nanoparticles which are probed in the Forced Rayleigh Scattering experiment (*i.e.* those of Table 1 of main paper or as well of Table 2 of E.S.I.) at $\lambda = 633$ nm. Core-shell NPs with a core of cobalt ferrite, of manganese ferrite and even with a core of mixed Zn-Mn ferrite are much more absorbing than pure maghemite NPs. They allow to perform Ludwig-Soret coefficient determinations in dispersions at volume fractions (here typically down to 0.4 %) lower than with maghemite nanoparticles (typically down to 1 %).

The optical indices of the dispersions are determined at $\lambda = 633$ nm with an Abbe refractometer. The measurements are presented as a function of the NP volume fraction at $T = 25°C$ for samples B6 and B7 in Fig. 2-a of E.S.I. and for sample B5 at $T = 10$ and $50°C$ in Fig. 2-b of E.S.I.. The NP's optical index is deduced from the Bruggeman model[5] (see section 2.2.2 of E.S.I.). We use for maghemite NPs the bulk value of maghemite (see Table 3 of E.S.I.), which is compatible with our measurements.

In order to determine experimentally the Ludwig-Soret coefficient $S_T$, it is necessary following Eq. 20 of main text to know

**Table 2** NP magnetic characteristics : "Sample" is the name of the sample family at various volume fractions, associated to the NPs on which the samples are based; Symbols used in most of the figures; "Ferrite core @ Surface group" denotes in the family, the core composition of the NPs and the chemical species on their surface; $m_s$ : magnetic magnetization of the NP material; Characteristics of the distribution of magnetic diameters $d^0_{mag}$ and $\sigma$ (see text); $d_{NP}$ : third moment of this distribution; Magnetic dipolar parameters $\Psi_{dd}$ and $\lambda_{max}$ characterizing respectively the particles and the dispersions (see text for formula); $\Phi_{max}$ is the maximal volume fraction of the samples probed here.

| Sample | Symbol | Ferrite core @ Surface group | $m_s$ (kA/m) | $d^0_{mag}$ (nm) | $\sigma$ | $d_{NP} = \sqrt[3]{\langle d^3_{mag}\rangle}$ (nm) | $\Psi_{dd}$ | $\Phi_{max}$ (%) | $\lambda_{max}$ |
|---|---|---|---|---|---|---|---|---|---|
| | | | *A-group* | | | | | | |
| A1 | △ | $\gamma$-$Fe_2O_3$ @ $Cit^{3-}$ | 310 | 9.8 | 0.25 | 10.8 | 34 | 10.3 | 0.28 |
| A2 | ◊ | | | | | | | 20 | 0.54 |
| A3 | ▽ | | | | | | | 15.3 | 0.41 |
| A4 | ▲ | | | 10 | 0.30 | 11.4 | 52 | 11.2 | 0.46 |
| A5 | ♦ | | | | | | | 15.4 | 0.64 |
| | | | *B-group* | | | | | | |
| B1 | ■ | $\gamma$-$Fe_2O_3$@ $H^+$ | 290 | 10 | 0.28 | 11.2 | 44 | 6 | 0.21 |
| B2 | × | | | 9 | 0.27 | 10.0 | 26 | 7.2 | 0.15 |
| B3 | + | | | 8.3 | 0.25 | 9.1 | 18 | 6.9 | 0.10 |
| B4 | ▼ | | | 7.5 | 0.20 | 8.0 | 10 | 4.4 | 0.04 |
| B5 | □ | $Mn_{0.23}Zn_{0.61}Fe_{1.94}O_4$@ $H^+$ | 237 | 9.6 | 0.38 | 11.9 | 58 | 2.3 | 0.11 |
| B6 | ● | $MnFe_2O_4$@ $H^+$ | 370 | 8.6 | 0.40 | 10.9 | 133 | 3.3 | 0.35 |
| B7 | ○ | $CoFe_2O_4$@ $H^+$ | 365 | 9.8 | 0.35 | 11.8 | 133 | 3.9 | 0.41 |

the ratio :

$$N_F = \frac{\partial n_{opt}/\partial \Phi}{\partial n_{opt}/\partial T} = \frac{\partial \varepsilon/\partial \Phi}{\partial \varepsilon/\partial T} \tag{1}$$

the dielectric constant $\varepsilon$ of the dispersion (at optical frequencies) being related to its optical index $n_{opt}$, through the relation :

$$\varepsilon = n^2_{opt}. \tag{2}$$

**Table 3** Optical characteristics (at 633 nm) of the nanoparticles probed in F.R.S.

| NPs | Optical absorption | Optical index $n_P$ |
|---|---|---|
| $A_i$ | 3.2 $10^5$ $m^{-1}$ | 2.6 |
| B1 to B4 | 3.3 $10^5$ $m^{-1}$ | 2.6 |
| B5 | 1.0 $10^6$ $m^{-1}$ | 2.4 |
| B6 | 2.0 $10^6$ $m^{-1}$ | 2.8 |
| B7 | 2.1 $10^6$ $m^{-1}$ | 2.8 |

### 2.2.2 Determination of $N_F$

In order to determine the coefficient $N_F$, let us begin with the Bruggeman equation from[5] relating $\varepsilon$ to the solvent dielectric constant $\varepsilon_S$ and the NP dielectric constant $\varepsilon_P$:

$$(1-\Phi)\frac{\varepsilon_S - \varepsilon}{\varepsilon_S + 2\varepsilon} + \Phi\frac{\varepsilon_P - \varepsilon}{\varepsilon_P + 2\varepsilon} = 0 \tag{3}$$

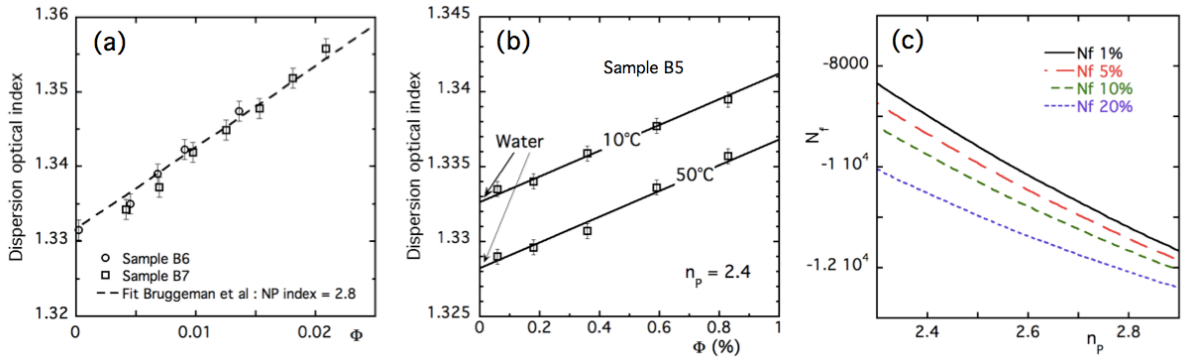


**Figure 2** (a) Optical index $n_{\text{opt}}$ of the dispersions as a function of the NP volume fraction $\Phi$ for samples B6 and B7 at $T = 25°\text{C}$. The dashed line is the Bruggemann model (see Eq. 4 of E.S.I.) with $n_P = 2.8$. (b) Optical index $n_{\text{opt}}$ of the dispersions as a function of the NP volume fraction $\Phi$ at $T = 10°\text{C}$ and $50°\text{C}$ for sample B5. The full line corresponds to the Bruggeman model (see Eq. 4 of E.S.I.) with $n_P = 2.4$. (c) Coefficient $N_F$ as a function of the optical index of the nanoparticles $n_p$ for various volume fractions $\Phi$ from 1% to 10 % as obtained from the formalism developed in section 2.2 of E.S.I..

We retain the positive root of this equation :

$$\varepsilon = \frac{1}{4}\,(2\varepsilon_{\text{S}} + \varepsilon_{\text{P}}) - \frac{3}{4}\,(\varepsilon_{\text{S}} + \varepsilon_{\text{P}}) + \frac{1}{4}\sqrt{(2\varepsilon + \varepsilon_{\text{P}})^2 - 6\Phi(2\varepsilon_{\text{S}} - \varepsilon_{\text{P}})(\varepsilon_{\text{S}} - \varepsilon_{\text{P}}) + 9\Phi^2(\varepsilon_{\text{S}} - \varepsilon_{\text{P}})^2)} \tag{4}$$

The optical index of the aqueous dispersions $n_{\text{opt}} = \sqrt{\varepsilon}$ is determined experimentally as a function of the NP volume fraction $\Phi$ (see figures 2-a and 2-b of E.S.I). The particle dielectric constant $\varepsilon_{\text{P}}$ (together with the particle optical index $n_{\text{P}} = \sqrt{\varepsilon_{\text{P}}}$) is obtained thanks to the fitting of $n_{\text{opt}}$ by Eq. 4. Table 3 of E.S.I. collects the $n_{\text{P}}$ values for all the samples of the main paper. For samples $\text{A}_i$ and B1-B4, $n_{\text{P}}$ is obtained close to the bulk refractive index of maghemite.

- The two derivatives $\partial\varepsilon/\partial T$ and $\partial\varepsilon/\partial\Phi$ of Eq. 1 are straighforwardly deduced from Eq.4.
- $\partial\varepsilon/\partial\Phi$ depends on $\varepsilon_{\text{S}}$, $\varepsilon_{\text{P}}$ and $\Phi$.
- $\partial\varepsilon/\partial T$ depends on $\varepsilon_{\text{S}}$, $\varepsilon_{\text{P}}$, $\Phi$ and their derivatives with respect to $T$: $\frac{\partial\varepsilon_{\text{S}}}{\partial T}$, $\frac{\partial\varepsilon_{\text{P}}}{\partial T}$, $\frac{\partial\Phi}{\partial T}$.
- we neglect $\partial\varepsilon_{\text{P}}/\partial T$ which is set here to 0, in first approximation.
- the dielectric constant $\varepsilon_{\text{S}}$ of the solvent and its derivative $\partial\varepsilon_{\text{S}}/\partial T$ are linked to the solvent index $n_{\text{S}}$ by :

$$\varepsilon_{\text{S}} = n_{\text{S}}^2 \quad \text{and} \quad \frac{\partial\varepsilon_{\text{S}}}{\partial T} = 2\,n_{\text{S}}\frac{\partial n_{\text{S}}}{\partial T} \tag{5}$$

The solvent is here water and we measure the temperature dependence of its refractive index at different pH values. Whatever the pH, the data are well described by the following expression from[6]:

$$\frac{\partial n_{\text{S}}}{\partial T} = -\,2.62\times10^{-4}\left(1 - e^{-(T-2)/48.5}\right) \tag{6}$$

where temperature $T$ is taken in °C. Taking $n_{\text{S}}$ = 1.332 at 23°C and $\lambda$ = 633 nm, leads to :

$$n_{\text{S}} = 1.3463 \;-\; 2.62\;10^{-4}\left(T + 48.5\,e^{-(T-2)/48.5}\right) \tag{7}$$

The volume fraction of nanoparticles can be written as $\Phi = V_P/(V_P + V_S)$ where $V_P$ and $V_S$ are respectively the total volume of nanoparticles and the total volume of water. If the dilatation of the nanoparticles is neglected, the derivative $\partial\Phi/\partial T$ is linked to the coefficient of thermal expansion of water:

$$A = \frac{1}{V_S}\frac{\partial V_S}{\partial T} \tag{8}$$

by the following relation :

$$\frac{\partial \Phi}{\partial T} = A\,\Phi\,(1-\Phi). \tag{9}$$

Equation (6) from reference[6] gives, by using the Lorentz model, the coefficient of thermal expansion of water $A$ as a function of the water dielectric constant $\varepsilon_S$:

$$A = -\frac{3}{(\varepsilon_S - 1)(\varepsilon_S + 2)}\frac{\partial \varepsilon_S}{\partial T}. \tag{10}$$

We thus obtain :

$$\frac{\partial \Phi}{\partial T} = \frac{3\Phi(1-\Phi)}{(\varepsilon_S - 1)(\varepsilon_S + 2)}\frac{\partial \varepsilon_S}{\partial T}. \tag{11}$$

Introducing $\varepsilon_S$, $\varepsilon_P$, $\Phi$, $\partial\varepsilon_P/\partial T = 0$, Eq. 7 and Eq. 11, in the derivatives $\partial\varepsilon/\partial\Phi$ and $\partial\varepsilon/\partial T$ of Eq. 4, we deduce the value of $N_F$ to be used to deduce the Ludwig-Soret coefficient $S_T$ in Eq. 20 of main text. Figure 2-c illustrates the $n_p$ and $\Phi$ dependences of the coefficient $N_F$ obtained here.

## 2.3 Soret coefficient

Figure 3 of E.S.I. presents the $\Phi$-dependence (and adjustment) of the Soret coefficient $S_T$ for the various samples of Table 1 from main paper, which are not presented in the plots of Fig. 2 of the main paper (except samples B1 and B5 where are re-plotted here). The $d_{NP}$-dependence of the effective number of charge $\xi_0$ associated to the best fits of Soret coefficient $S_T$ are presented in Fig. 4 of E.S.I.. This figure shows that these $\xi_0$ values scales as the NP's surface.

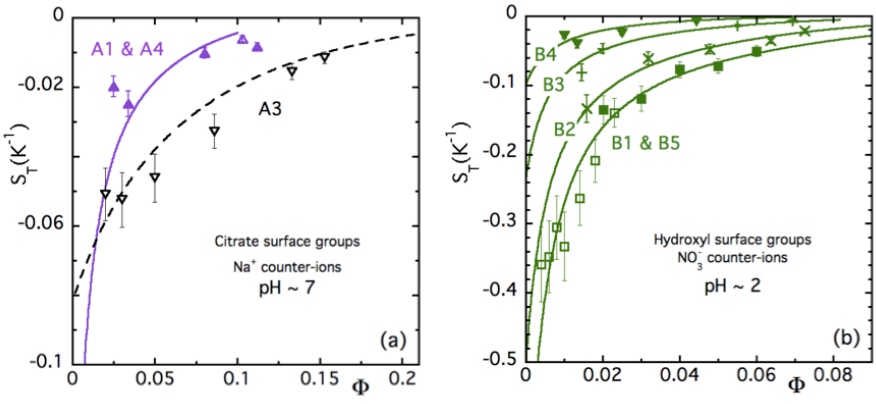


**Figure 3** Soret coefficient $S_T$ as a function of the NP volume fraction $\Phi$ for some samples of Table 1 of main paper. Various lines are best fits of the data using Eq. 3, 7, 17 and 22 of the main paper.

## 2.4 Hydrodynamic characteristics at T = 22.5 °C

In the Forced Rayleigh Scattering experiment, the mass diffusion coefficient $D_m$ is determined (in the absence of temperature gradient) through the relaxation of the diffracted intensity $I_{dif}$ at the cut-off of the pump beam, thus at the relaxation of the spatial modulations of concentration (at wavelength $\Lambda$) induced in the sample by the Soret effect. The $I_{dif}(t)$ relaxation is exponential with a characteristic relaxation time $\tau$ which is inversely proportional to the square of the scattering vector $q = 2\pi/\Lambda$. This point

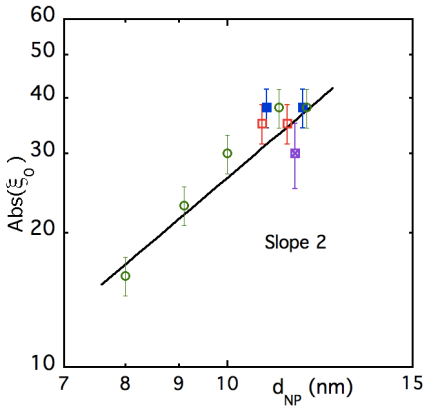


**Figure 4** Log-log representation of the absolute value of the effective charge number $|\xi_0|$ associated with the experimental adjustment of $S_T$ by Eq.(17) as a function of the NP diameter $d_{\mathrm{NP}}$. Full line corresponds to $\xi_0 \propto d_{\mathrm{NP}}^2$ and symbols : (open red square : samples of A-group at $pH = 7$; green open circle : samples B1 to B5 at $pH = 2$; blue filled square : samples B6 & B7 at $pH = 2.5$; purple cross-in-a-square : sample A-$NO_3^-$-W at $pH = 1.7$ from reference[7])

is illustrated by Fig. 5 of E.S.I. for sample B1 at $\Phi = 0.4\%$. $D_{\mathrm{m}}$ is the coefficient of proportionality between $\tau^{-1}$ and $q^2$. Fig. 3 of main paper shows the whole measurements. The FRS measurements are complemented by Quasi-Elastic Light Scattering (Q.E.LS.) measurements of $D_{\mathrm{m}}$ at low volume fractions ($\Phi \sim 10^{-2}\%$) with a Malvern NanoZS. Whatever the sample, $D_{\mathrm{m}}$ linearly increases with $\Phi$ in the probed $\Phi$-range, demonstrating that the interparticule interaction is repulsive on average at $T = 22.5°\mathrm{C}$. Table 4 of E.S.I. collects the values $D_{\mathrm{m},0}$ of $D_{\mathrm{m}}$, extrapolated at $\Phi = 0$ , the friction coefficient $\zeta_0$ and the hydrodynamic radius $R_{\mathrm{H}}$ of the NPs deduced from :

$$D_{\mathrm{m},0} = \frac{kT}{\zeta_0} = \frac{kT}{6\pi\eta R_{\mathrm{H}}} \tag{12}$$

$\eta$ being the solvent viscosity.

**Table 4** Hydrodynamic characteristics deduced at $\Phi = 0$ from RFS ans QELS measurements for the samples from Table 1 of main paper at $T = 22.5 \pm 0.5$ °C (see the text) of section 2.4 of E.S.I..

| Sample | $D_{\mathrm{m},0}$ ($10^{-11}$ m$^2$/s) | $\zeta_0$ ($10^{-10}$ J s m$^{-2}$) | $R_{\mathrm{H}}$ (nm) |
|---|---|---|---|
| $A_i$ | 2.87 | 1.39 | 8.1 |
| B1 | 2.06 | 1.94 | 11.3 |
| B2 | 2.3 | 1.74 | 10.1 |
| B3 | 2.5 | 1.6 | 9.3 |
| B4 | 3 | 1.33 | 7.7 |
| B5 | 1.97 | 2.14 | 11.8 |
| B6 | 2.04 | 1.9 | 11.4 |
| B7 | 2.02 | 1.9 | 11.5 |

## 2.5 Effective charge determination as a function of temperature

The temperature-dependence of the dynamic effective charge $e\xi_0$ is determined thanks to the measurement as a function of temperature $T$ of :

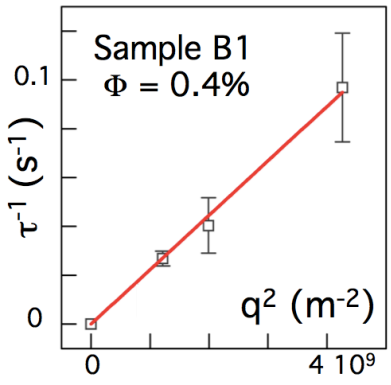


**Figure 5** Inverse of relaxation time $\tau^{-1}$ versus $q^2$, the square of the scattering vector, for sample B1 at $\Phi = 0.4\%$.

- $\mu_0^{\rm el}$, the electrophoretic mobility of the NPs in very dilute colloidal dispersions (at $\Phi \sim 0.01\%$) using a Nano ZS associated with a dip cell from Malvern,
- $D_{\rm m,0}$, the diffusion coefficient at zero concentration using a Vasco DLS particle analyzer from Cordouan Technologies dedicated to dark media, at a volume fraction $\Phi \sim 0.2\%$.

The two devices are thermalized and both operate typically between 15 and 40 °C. The number $\xi_0$ of dynamic effective charge is deduced from these measurements, using the following expression:

$$\xi_0 = \frac{kT\mu_0^{\rm el}}{e\,D_{\rm m,0}}. \tag{13}$$

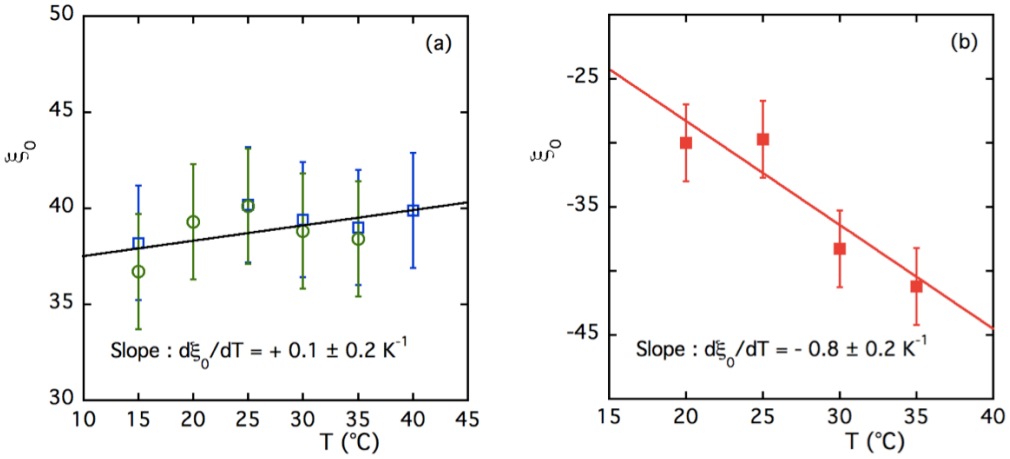


**Figure 6** Temperature dependence of the dynamic effective number of charge $\xi_0$ for various dispersions : (a) NPs coated with hydroxyl groups at $pH = 2$ (open green circles) and $pH = 3$ (open blue squares) with $NO_3^-$ counterions (sample B10 of Table1 of E.S.I) and (b) citrate-coated NPs at $pH = 7$ (filled red squares) with $Na^+$ counterions at $[Na^+]_{\rm free}$= 8. $10^{-2}$ mol/L (NPs are slightly smaller but more polydisperse than NPs from A-group of main paper) - color on line

Two kinds of samples are here probed.

- Sample B10 from Table 1 of E.S.I. is a sample with NPs coated with hydroxyl groups. The NPs are dispersed in acidic aqueous media with $NO_3^-$ counter-ions. The number of charge $\xi_0$ is determined here both at pH $=$ 2 and pH $=$ 3 for $T$ ranging from 15°C to 40°C. As illustrated by Fig. 6.a of E.S.I. the number $\xi_0$ of dynamic effective charge is positive in that case. It does not depend on pH (in the range of the experiment and within its error bar) and we obtain $d\xi_0/dT = +0.1 \pm 0.2$ K$^{-1}$ for these acidic dispersions.

- Another sample, with citrate coated NPs dispersed at pH $=$ 7 thanks to $Na^+$ counterions at $[Na^+]_{free} = 8 \times 10^{-2}$ mol/L is probed here for $T$ ranging between 20°C and 35°C. This sample is comparable to samples $A_i$ of main paper, with a slightly smaller size and a larger polydispersity. The measured number of charge $\xi_0$ is presented in Fig. 6.b of E.S.I. as a function of $T$. It is negative and decreases (in algebraic values) as $d\xi_0/dT = -0.8 \pm 0.2$ K$^{-1}$.

## 2.6 NP's Eastman entropy of transfer

$\hat{S}_{NP}$, the Eastman entropy of transfer of the nanoparticles (deduced from the adjustment of $S_T(\Phi)$ – see the main paper) is plotted in Fig. 7 as a function of :

- *the screening length* $\kappa^{-1}$ *at roughly constant* $d_{NP}$ in figures 7.a and 7.b (for samples with $d_{NP}$ ranging between 10.8 nm and 11.9 nm). Fig. 7.a corresponds to samples with citrate-coated NPs and $Na^+$ counter-ions (samples of A-group at pH $=$ 7 from Table 1 of main paper) and Fig. 7.b to samples with hydroxyl-coated NPs and $NO_3^-$ counter-ions (samples of B-group at pH $=$ 2 and 2.5 from Table 1 of main paper, plus sample A–$NO_3^-$–W at pH $=$ 1.7 from reference [7]).

- *the NP's surface at constant* $\kappa^{-1}$ (= 3.2 nm) in Fig. 7.c, for acidic samples at pH $=$ 2 of Table 1 of main paper (hydroxyl-coated NPs and $NO_3^-$ counter-ions).

These two dependencies of $\hat{S}_{NP}$ are regrouped as a function of the reduced parameter $\pi d_{NP}^2 \kappa^{-1}$ in Fig. 4 of main paper. For a given NP-coating, $\hat{S}_{NP}$ depends linearly the (at the first order) on the volume of the electrostatic double layer.

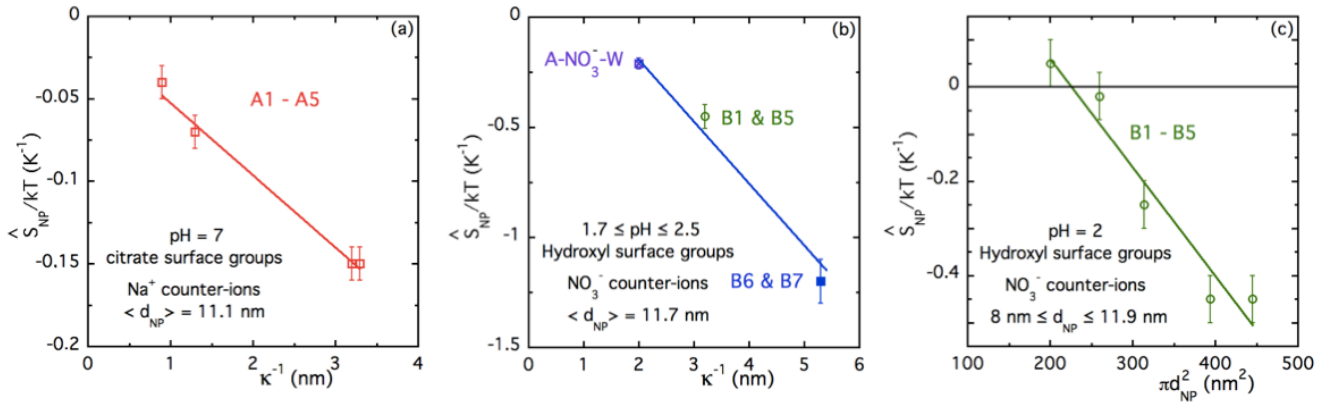


**Figure 7** NP's Eastman entropy of transfer $\hat{S}_{NP}$ of various samples **– (a) and (b) plotted as a function of the screening length** $\kappa^{-1}$ at roughly constant $d_{NP}$; **(a) samples** $A_i$ (citrate-coated NPs with $Na^+$ counter-ions and $\langle d_{NP} \rangle \sim 11.1$ nm) and **(b) samples of B-group** from Table 1 of the main paper (with hydroxyl-coated NPs and $NO_3^-$ counter-ions) at $\langle d_{NP} \rangle \sim 11.7$ nm and various pH (blue filled square : samples B6 & B7 at pH $=$ 2.5, green open circle : samples B1 & B5 at pH $=$ 2, purple cross-in-a-square : sample A-$NO_3^-$-W at pH $=$ 1.7 from reference [7]). **– (c) plotted as a function of the NP's surface** for samples B1-B5 at pH $=$ 2 (with hydroxyl-coated NPs and $NO_3^-$ counter-ions) – Various lines are linear guides for the eyes of the data – see main text for a regrouping of these dependencies.

# 3 The capacitor model

In the capacitor model, the driving force of thermodiffusion is the variation of free energy due to the buildup of the electrostatic double layer around the charged nanoparticles of radius $R_{\rm NP}$. It is seen as a spherical capacitor of thickness equal to the screening length $\kappa^{-1}$ and radius $R_{\rm NP}$ with a stored energy $W$ [8,9]. The capacitor-model contribution $\hat{S}_{\rm NP}^{\rm CM}$ to $\hat{S}_{\rm NP}$ writes as :

$$\frac{\hat{S}_{\rm NP}^{\rm CM}}{kT} = \frac{1}{kT}\frac{\partial W}{\partial T} \quad \text{with} \quad W = \frac{(e\xi_0)^2}{2\pi\varepsilon_0\varepsilon(T)d_{\rm NP}(2+\kappa d_{\rm NP})} \tag{14}$$

with $\varepsilon(T)$ the relative permittivity of water.

If the effective charge number $\xi_0$ does not depend on temperature, $\hat{S}_{\rm NP}^{\rm CM}$ reduces to $\hat{S}_{\rm NP}^{\rm CM,a}$, which equals [9] :

$$\frac{\hat{S}_{\rm NP}^{\rm CM,a}}{kT} = \frac{(e\xi_0)^2}{4\pi\varepsilon_0\varepsilon(T)kT^2\kappa^{-1}(2+\kappa d_{\rm NP})^2}\left[1-\frac{\partial\ln\rho}{\partial\ln T}-\frac{\partial\ln\varepsilon}{\partial\ln T}\left(1+\frac{4}{\kappa d_{\rm NP}}\right)\right] \tag{15}$$

where we have been using

$$\frac{\partial\kappa^{-1}}{\partial T} = \frac{\kappa^{-1}}{2T}\left[1-\frac{\partial\ln\rho}{\partial\ln T}+\frac{\partial\ln\varepsilon}{\partial\ln T}\right] \tag{16}$$

$\rho$ being the density of water.

If the effective charge number $\xi_0$ depends on temperature, $\hat{S}_{\rm NP}^{\rm CM}$ contains an extra contribution $\hat{S}_{\rm NP}^{\rm CM,b}$ :

$$\frac{\hat{S}_{\rm NP}^{\rm CM,b}}{kT} = \frac{e^2\ \xi_0\ \partial\xi_0/\partial T}{\pi\varepsilon_0\varepsilon(T)kT\,d_{\rm NP}(2+\kappa d_{\rm NP})} \tag{17}$$

These two contributions $\frac{\hat{S}_{\rm NP}^{\rm CM,a}}{kT}$ and $\frac{\hat{S}_{\rm NP}^{\rm CM,b}}{kT}$, together with their sum :

$$\frac{\hat{S}_{\rm NP}^{\rm CM}}{kT} = \frac{\hat{S}_{\rm NP}^{\rm CM,a}}{kT} + \frac{\hat{S}_{\rm NP}^{\rm CM,b}}{kT} \tag{18}$$

are plotted in Figure 6 of main paper for A-group samples (with citrate coated NPs at pH $=$ 7) and those at pH $=$ 2 from B-group samples (with NPs coated with hydroxyl groups). We have used $\frac{\partial\ln\rho}{\partial\ln T} = -0.07$ and $\frac{\partial\ln\varepsilon}{\partial\ln T} = -1.34$ from [8] for these aqueous samples at $T = 22.5°$C.

# References


[1] G. Mériguet, F. Cousin, E. Dubois, F. Boué, A. Cēbers, B. Farago and R. Perzynski, *J. Phys. Chem. B*, 2006, **110**, 4378–4386.

[2] G. Mériguet, E. Wandersman, E. Dubois, A. Cēbers, J. Gomes, G. Demouchy, J. Depeyrot, A. Robert and R. Perzynski, *Magnetohydrodynamics*, 2012, **48**, 415–425.

[3] E. Wandersman, A. Cēbers, E. Dubois, G. Mériguet, A. Robert and R. Perzynski, *Soft Matter*, 2013, **9**, 11480–11489.

[4] *Magnetic Fluids and Applications Handbook*, ed. B. Berkovski, Begell House Inc. Publ., N.Y., 1996.

[5] D. Bruggeman, *Ann. Phys., ser. 5*, 1935, **24**, 636–679.

[6] G. Abbate, U. Bernini, E. Ragozzino and F. Somma, *J. Phys. D: Appl. Phys.*, 1978, **11**, 1167–1172.

[7] C. L. Filomeno, M.Kouyaté, V. Peyre, G. Demouchy, A. Campos, R. Perzynski, F. Tourinho and E. Dubois, *J. Phys. Chem. C*, 2017, **121**, 5539–5550.

[8] J. Dhont, S. Wiegand, S. Duhr and D. Braun, *Langmuir*, 2007, **23**, 1674–1683.

[9] M. Reichl, M. Herzog, A. Gotz and D. Braun, *Phys. Rev. Lett.*, 2014, **112**, 198101 pp.1–5.